AGU PUBLICATIONS

JGR

Journal of Geophysical Research: Atmospheres

RESEARCH ARTICLE
10.1002/2015JD023999

This article is a companion to *Matsui* [2016] doi:10.1002/2015JD023998.

Key Points:
- Simulation of the aging timescale and CCN activity of BC by a 2-D aerosol bin model (12 × 10 bins)
- These BC parameters are shown three dimensionally with the large size/supersaturation dependence
- Importance of resolving BC mixing state for simulations of BC and its CCN activity is shown

Correspondence to:
H. Matsui,
matsui@nagoya-u.jp

Citation:
Matsui, H. (2016), Black carbon simulations using a size- and mixing-state-resolved three-dimensional model: 2. Aging timescale and its impact over East Asia, *J. Geophys. Res. Atmos.*, *121*, 1808–1821, doi:10.1002/2015JD023999.

Received 27 JUL 2015
Accepted 19 DEC 2015
Accepted article online 23 DEC 2015
Published online 20 FEB 2016

Black carbon simulations using a size- and mixing-state-resolved three-dimensional model: 2. Aging timescale and its impact over East Asia

H. Matsui[1,2,3]

[1]Graduate School of Environmental Studies, Nagoya University, Nagoya, Japan, [2]Department of Earth and Atmospheric Sciences, Cornell University, Ithaca, New York, USA, [3]Department of Environmental Geochemical Cycle Research, Japan Agency for Marine-Earth Science and Technology, Yokohama, Japan

Abstract This study evaluates the aging timescale and the cloud condensation nuclei (CCN) activity of black carbon (BC) over East Asia and its outflow region using a size- and mixing-state-resolved three-dimensional model, the Weather Research and Forecasting model with chemistry (WRF-chem) with the Aerosol Two-dimensional bin module for foRmation and Aging Simulation (ATRAS) and the Model for Simulating Aerosol Interactions and Chemistry (MOSAIC). The WRF-chem/ATRAS-MOSAIC model explicitly calculates BC aging (condensation and coagulation) and removal processes, with 12 size and 10 BC mixing state bins (128 bins in total). The model reveals large spatial and temporal variability of the BC aging timescale and the CCN activity of BC-containing particles over East Asia (spring 2009) with their strong size and supersaturation dependence. The BC aging timescale differs from 0.19 to 3.1 days (period and domain average at an altitude of 1 km), depending on the choice of size (mass or number) and supersaturation (1.0% or 0.1%). As a result, almost 100% of BC-containing particles are CCN-active at a supersaturation of 1.0%, whereas 20–50% of BC-containing particles are CCN-inactive at a supersaturation of 0.1%, with a strong size dependence. These results show the importance of resolving BC aging processes and their dependence on size and supersaturation in models for more accurate simulations of BC concentrations and their distribution and lifetime. A sensitivity simulation without resolving BC mixing state shows the underestimation of total BC mass concentrations by 5–10% and the BC mass concentrations in the CCN-inactive particles (at a supersaturation of 0.1%) by 40–60% over the outflow region (at 150°E), compared with the simulation resolving BC mixing state. Because BC aging speed is very slow at 150°E and eastward, the change in BC mass and its CCN activity by resolving BC mixing state will continue over long distances and may have a large impact on BC transport from East Asia to remote regions such as North America and the Arctic.

1. Introduction

Black carbon (BC) is emitted mainly from the incomplete combustion of fossil fuels, biofuels, and biomass burning. BC particles are considered to contribute to the warming of Earth's atmosphere by strongly absorbing solar radiation [*Ramanathan et al.*, 2001; *Bond et al.*, 2013], and the direct effect is estimated to have a large positive radiative forcing [*Boucher et al.*, 2013; *Myhre et al.*, 2013]. BC absorption is also thought to affect cloud formation processes by modifying the vertical stability of the atmosphere [*Johnson et al.*, 2004; *Koch and Del Genio*, 2010]. In addition, BC particles change cloud microphysical properties indirectly by acting as cloud condensation nuclei (CCN) [*Chen et al.*, 2010]. Furthermore, BC particles have the potential to reduce snow albedo when they are transported long distances and deposited onto the surface of snow and ice [*Hansen and Nazarenko*, 2004]. Despite the importance of BC in climate, BC model simulations are still very uncertain and diverse, especially over remote regions such as the Arctic [*Shindell et al.*, 2008; *Koch et al.*, 2009].

BC microphysical and chemical properties are gradually changed in the atmosphere by aging processes such as condensation, coagulation, and/or photochemical oxidation [*Riemer et al.*, 2009; *Oshima et al.*, 2009]. BC particles just after emission are generally less CCN-active, but they are gradually coated by non-BC species and become more CCN-active during transport. Because the enhancement of CCN activity increases the wet removal rate of BC and reduces the lifetime of BC, the aging processes are important to simulate BC concentrations and distributions in the atmosphere [*Croft et al.*, 2005; *Stier et al.*, 2006]. Most three-dimensional models represent the change in the CCN activity of BC by a conversion rate (aging timescale) from hydrophobic (CCN-inactive) to hydrophilic (CCN-active). The aging timescale was originally treated as

a constant value (e.g., 24 h) [e.g., *Cooke et al*., 2002], but it is now treated as a variable in many models, with a dependence on sulfuric acid and/or aerosol number concentrations [*Riemer et al*., 2004; *Liu et al*., 2011; *Oshima and Koike*, 2013]. Some global modeling studies have shown that the treatment of BC aging processes and the resulting wet removal processes are important factors for realistic simulation of BC concentrations over Arctic regions [*Liu et al*., 2011; *Huang et al*., 2010].

Box modeling studies treat the BC aging processes in more detail by resolving the microphysical and chemical properties of BC [*Riemer et al*., 2009, 2010; *Oshima et al*., 2009; *Zaveri et al*., 2010; *Fierce et al*., 2015]. For example, *Riemer et al*. [2009] have developed a stochastic particle-resolved model, which explicitly resolves the size and the composition of individual particles. They simulated the evolution of the BC mixing state by condensation and coagulation in an idealized urban plume and showed that condensation (coagulation) dominated the aging processes during the daytime (nighttime) [*Riemer et al*., 2010]. In addition, they found a strong dependence of the BC aging timescale on supersaturation (e.g., 0.1% or 1%). *Oshima et al*. [2009] and *Zaveri et al*. [2010] have shown the importance of resolving the size and mixing state of BC for more accurate simulations of the CCN activity of BC-containing particles.

These box models are useful for understanding the BC aging processes in a plume. However, to my knowledge, no previous studies have evaluated the spatial distributions of the BC aging timescale by using a three-dimensional model that adequately resolves the size and mixing state of aerosols. There is still a large gap in the representation of BC aging processes between zero-dimensional (box) models and three-dimensional (global) models.

Matsui et al. [2013a, 2014a] developed and validated a size- and BC-mixing-state-resolved three-dimensional aerosol model. The model, which is called the Aerosol Two-dimensional bin module for foRmation and Aging Simulation (ATRAS), calculates BC aging processes by condensation and coagulation with 12 size bins (dry diameter from 40 nm to 10 μm) and 10 BC mixing state bins. Therefore, the ATRAS model resolves pure BC, BC-free, and eight different internally mixed particles for each size bin. The model successfully reproduced some important features of the BC mixing state observed by a single particle soot photometer [*Matsui et al*., 2013a].

Part 1 of this paper evaluated BC absorption and radiative effect and their uncertainties over East Asia using the ATRAS model [*Matsui*, 2016]. In part 2 (this paper), the focus is the CCN activity of BC-containing particles. The aging timescale and the microphysical properties of BC (e.g., the fraction of CCN-active and CCN-inactive BC particles) are evaluated three-dimensionally by using a size- and mixing-state-resolved model. Following the description of the ATRAS model (section 2) and the simulation setups (section 3), this study evaluates the spatial distributions of the BC aging timescale and its strong dependence on size and supersaturation over East Asia and its outflow region (section 4.1). Then, this study shows the impact of the BC aging timescale on the CCN activity of BC (the fraction of CCN-inactive BC particles) over the region, including its dependence on size and supersaturation (section 4.2). Finally, sensitivity simulations with and without resolving BC mixing state show the importance of resolving the BC mixing state in the model for more accurate simulations of BC and its CCN activity over East Asia and its outflow regions (section 4.5).

2. Size- and Mixing-State-Resolved Model

2.1. WRF-Chem/ATRAS-MOSAIC

Because the treatment of aerosols in the ATRAS module has been described in previous papers [*Matsui et al*., 2013a, 2014a] and part 1 [*Matsui*, 2016] in detail, this paper discusses them only briefly. The ATRAS module developed by *Matsui et al*. [2014a] uses the framework of the Weather Research and Forecasting model with chemistry (WRF-chem) version 3.4 [*Grell et al*., 2005; *Skamarock et al*., 2008] and the Model for Simulating Aerosol Interactions and Chemistry (MOSAIC) aerosol module [*Fast et al*., 2006; *Zaveri et al*., 2008]. The ATRAS module uses 128 aerosol bins (8 size bins from 1 to 40 nm and 12 size × 10 mixing state bins from 40 nm to 10 μm in dry diameter) for each of the aerosol-phase and cloud-phase particles. The module therefore uses 256 aerosol bins in total, as shown in Figure 1 of part 1. The module calculates mass concentrations of sulfate, nitrate, ammonium, organics, BC, dust, sodium, chloride, and aerosol water and number concentrations for each aerosol bin. The aerosol microphysical and chemical processes considered in the ATRAS module are emissions of aerosol and gaseous species, nucleation at 1 nm [*Matsui et al*., 2011a, 2013b] by the activation

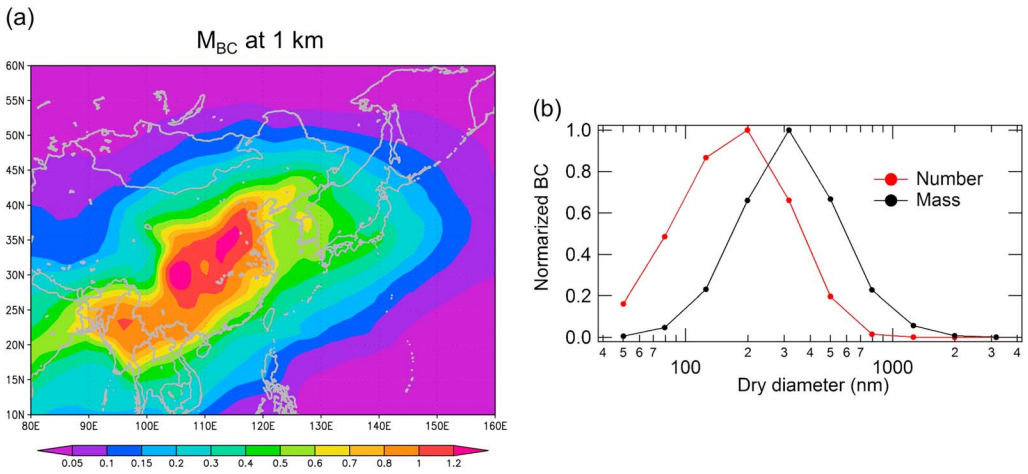

Figure 1. (a) BC mass concentrations ($\mu g\ m^{-3}$) at a sigma level of 0.895 (~1 km) during the simulation period. The mean concentrations are calculated for the model results from 24 March to 26 April 2009. (b) The period- and domain-averaged normalized size distributions for number concentrations of BC-containing particles (red) and for BC mass concentrations (black) at an altitude of 1 km. Particle size shows the dry diameter for total aerosols, including both BC and non-BC species (not BC diameter).

mechanism [*Kulmala et al.*, 2006], condensation/evaporation of inorganic species [*Zaveri et al.*, 2008] for the two-dimensional bins [*Matsui et al.*, 2013a], condensation/evaporation of organic species by the volatility basis set approach [*Matsui et al.*, 2014b], shifts of bins by condensation/evaporation for the size dimension [*Simmel and Wurzler*, 2006] and the mixing state dimension [*Jacobson*, 1997], coagulation within the two-dimensional bins [*Matsui et al.*, 2013a], aerosol activation to cloud and evaporation from cloud [*Abdul-Razzak and Ghan*, 2000], aqueous-phase chemistry in the cloud phase [*Fahey and Pandis*, 2001], and dry deposition and in-cloud and below-cloud scavenging [*Easter et al.*, 2004].

The CCN activity of BC-containing particles is calculated by using the k-Köhler theory [*Petters and Kreidenweis*, 2007] at supersaturations of 1% and 0.1%. The volume-averaged hygroscopicity parameters (κ) are calculated for each aerosol bin by using κ values of 1.16 for sodium and chloride, 0.5 for sulfate, ammonium, and nitrate, 0.14 for organics and dust, and 1×10^{-6} for BC. The critical supersaturation is calculated from the particle size and the κ value for each bin [*Matsui et al.*, 2011a], and it is used to evaluate whether the particles in each aerosol bin are CCN-active or CCN-inactive at supersaturations of 1% and 0.1%.

2.2. Definition of the BC Aging Timescale

The framework of the BC aging timescale was introduced by *Riemer et al.* [2010]. The BC aging timescale is calculated for both mass and number concentrations and for both condensation and coagulation processes as follows:

$$\tau_{M,\mathrm{cond}}(x,y,z,t,s) = \frac{M_{\mathrm{inact}}(x,y,z,t,s)}{\Delta M_{\mathrm{cond}}(x,y,z,t,s)/\Delta t} \tag{1a}$$

$$\tau_{M,\mathrm{coag}}(x,y,z,t,s) = \frac{M_{\mathrm{inact}}(x,y,z,t,s)}{\Delta M_{\mathrm{coag}}(x,y,z,t,s)/\Delta t} \tag{1b}$$

$$\tau_{N,\mathrm{cond}}(x,y,z,t,s) = \frac{N_{\mathrm{inact}}(x,y,z,t,s)}{\Delta N_{\mathrm{cond}}(x,y,z,t,s)/\Delta t} \tag{1c}$$

$$\tau_{N,\mathrm{coag}}(x,y,z,t,s) = \frac{N_{\mathrm{inact}}(x,y,z,t,s)}{\Delta N_{\mathrm{coag}}(x,y,z,t,s)/\Delta t}, \tag{1d}$$

where $\tau_{M,p}$ ($\tau_{N,p}$) is the BC aging timescale for mass (number) concentrations for process p (condensation or coagulation) on a three-dimensional grid x, y, and z, at time t, and at supersaturation s (1.0% or 0.1%); M_{inact} is the BC mass concentration in CCN-inactive particles; N_{inact} is the number concentration of CCN-inactive BC-containing particles; ΔM_p is the BC mass concentration changed from CCN-inactive to CCN-active by process p; ΔN_p is the number concentration of BC-containing particles changed from CCN-inactive to CCN-active by process p; and Δt is the model time step. The values of M_{inact} and N_{inact} are calculated

for particles before the calculations of each process (condensation or coagulation) in the model. A shift of size and/or mixing state bins by condensation is calculated by a two-moment advection method (for size bins) and the moving center approach (for mixing state bins) (section 2.1). The values of ΔM_{cond} and ΔN_{cond} are calculated on the basis of the particles experiencing bin shifts from a CCN-inactive bin to a CCN-active bin in a time step by tracing all the combinations of aerosol bins before and after calculation of the bin shifts due to condensation. In the calculations of coagulation, the production of a particle in bin k from two particles in bins i and j is traced for all the combinations of aerosol bins i, j, and k. When a produced particle (in bin k) is CCN-active and either or both of the lost particles (in bins i and/or j) are CCN-inactive, the BC mass in the CCN-inactive particles is treated as ΔM_{coag}. When a produced particle is CCN-active and both lost particles are CCN-inactive, the produced particle is treated as ΔN_{coag}. The total BC aging timescale (the sum of condensation and coagulation processes) is calculated as follows:

$$\frac{1}{\tau_M(x,y,z,t,s)} = \frac{1}{\tau_{M,\mathrm{cond}}(x,y,z,t,s)} + \frac{1}{\tau_{M,\mathrm{coag}}(x,y,z,t,s)} \tag{2a}$$

$$\frac{1}{\tau_N(x,y,z,t,s)} = \frac{1}{\tau_{N,\mathrm{cond}}(x,y,z,t,s)} + \frac{1}{\tau_{N,\mathrm{coag}}(x,y,z,t,s)}, \tag{2b}$$

where τ_M and τ_N are the total BC aging timescales for BC mass concentrations and the number concentrations of BC-containing particles, respectively.

In this study, a spatial and/or period average of the BC aging timescale is defined as the ratio between an average of the numerator (e.g., M_{inact}) and an average of the denominator (e.g., $\Delta M_{\mathrm{coag}}/\Delta t$) in equation (1) (not the average of the BC aging timescales).

The BC aging timescale is evaluated for BC number (number concentrations of BC-containing particles) at supersaturations of 1.0% (SS1.0 N) and 0.1% (SS0.1 N) and BC mass at a supersaturation of 0.1% (SS0.1 M). The aging timescale for BC mass at a supersaturation of 1.0% is not evaluated because M_{inact} is too small (M_{inact} was about 0.1% of total BC mass) at this supersaturation in the simulations shown in this study.

Because nitrate and organics are calculated in the ATRAS-MOSAIC model, it is possible for their evaporation to change some BC particles from CCN-active to CCN-inactive. However, changes due to evaporation are not considered in the calculations of the BC aging timescale in this study. Only one-way changes in CCN activity (from CCN-inactive to CCN-active) are considered in the calculations of the BC aging timescale.

2.3. Definition of the CCN-Inactive BC Fraction

The CCN-inactive fractions of the BC mass concentrations and the number concentrations of BC-containing particles are calculated in the model after the calculations of condensation and coagulation in each time step by

$$F_M(x,y,z,t,s) = \frac{M_{\mathrm{inact}}(x,y,z,t,s)}{M(x,y,z,t,s)} \tag{3a}$$

$$F_N(x,y,z,t,s) = \frac{N_{\mathrm{inact}}(x,y,z,t,s)}{N(x,y,z,t,s)}, \tag{3b}$$

where F_M and F_N are the CCN-inactive fractions of BC mass and number, respectively; M is the total BC mass concentration; and N is the number concentration of BC-containing particles (both CCN-active and CCN-inactive particles).

Similar to the BC aging timescale, the CCN-inactive fractions are calculated for SS1.0 N, SS0.1 N, and SS0.1 M. An average of the CCN-inactive fraction is defined as the ratio of an average of the numerator (e.g., M_{inact}) to an average of the denominator (e.g., M) in equation (3).

3. Simulation Setups

The simulation domains and periods are the same as those used in part 1 of this paper [*Matsui*, 2016] and in previous studies [*Matsui et al.*, 2013a, 2014a]. Two domains are used in this study: the outer domain covers East Asia (including China and India) and the western Pacific, and the inner domain covers China, Korea, and Japan (Figure 3 of part 1). In this study, the results of both domains are used in the analysis. The simulation periods are from 21 March to 26 April 2009. As noted in part 1, the simulations have previously been

validated for various aerosol parameters, such as the mass concentrations of BC, sulfate, and organics, aerosol number concentrations (>10 nm in diameter), and BC mixing states [*Matsui et al*., 2013a, 2013b, 2014a, 2014b] by using aircraft and surface measurements [*Takami et al*., 2005, 2007; *Kondo et al*., 2011; *Oshima et al*., 2012; *Moteki et al*., 2012] during the simulation periods. The emission inventories are also similar to those used in part 1 and in previous studies: the anthropogenic and volcanic emissions of *Streets et al*. [2003], biomass burning emissions of the Global Fire Emissions Database version 3 [*van der Werf et al*., 2010], and biogenic emissions of the Model of Emissions of Gases and Aerosols from Nature version 2 [*Guenther et al*., 2006]. The size distribution and the mixing state of aerosol emissions are the same as those in the base simulation in part 1: the number median diameter is 70 nm for fossil fuel sources and 150 nm for biofuel and biomass burning sources with a standard deviation of 1.8 and 50% of the BC is assumed to be externally mixed. All aerosol emissions are treated as particles from 40 nm to 10 μm in dry diameter, as described in part 1. The main conclusions obtained in this study are not changed by the treatment of emitted particles less than 40 nm in dry diameter.

4. Simulation Results

4.1. BC Aging Timescale

Figure 1a shows the period-averaged BC mass distribution at an altitude of 1 km. The distribution of BC mass concentrations generally corresponds to that of BC emissions, and the concentrations are high over China and Southeast Asia. Figure 1b shows the average size distributions of BC mass concentrations and the number concentrations of BC-containing particles (period and domain average at an altitude of 1 km). The size distributions are shown for dry diameters of all species (including both BC and non-BC species). The size distributions have a maximum at 200 nm for BC number and at 300 nm for BC mass. This study evaluates the BC aging timescale (section 4.1) and the CCN-inactive BC fraction (section 4.2) in terms of both mass and number concentrations. A fundamental difference between mass-based and number-based BC aging timescales is the representative diameters of BC-containing particles, as shown in Figure 1b. The BC aging timescale for mass (number) reflects the timescale for larger (smaller) BC-containing particles.

Figure 2 shows the distributions of the BC aging timescales at an altitude of 1 km for SS1.0 N, SS0.1 N, and SS0.1 M for both condensation and coagulation processes. Overall, the distribution of the BC aging timescale is similar for all parameters: the timescale is lower (the aging speed is faster) near the source regions and higher (slower) over the outflow regions. The aging speed slows by 2 orders of magnitude during transport from the source areas to the outflow regions. The distributions of the BC aging timescale differed somewhat between condensation and coagulation. The distribution of the timescale for coagulation reflects the distribution of aerosol concentrations, and the contrast between the source areas and the outflow regions is clearer for coagulation than for condensation (Figures 2d–2f). In contrast, the BC aging timescale for condensation is small, not only over the source areas but also over the outflow regions such as Japan, where the concentrations and/or the fractions of secondary species are high (Figures 2a–2c). These differences may be explained by the parameters dominating condensation and coagulation equations: the ratio of secondary aerosol formation rate to the concentrations of preexisting particles is important for condensation, whereas aerosol number concentrations are important for coagulation. The BC aging timescale for condensation has larger spatial variability than that for coagulation: the range of the BC aging timescale for SS1.0 N is 0.5–23.5 days for condensation and 1.13–18.3 days for coagulation within the region shown in Figure 2.

The absolute values of the BC aging timescale differed greatly between the parameters. The BC aging timescale for SS1.0 N is 0.21 day for condensation and 2.8 days for coagulation (period and domain average), whereas the timescales for SS0.1 N are 4.6 days for condensation and 9.5 days for coagulation (Table 1). In addition, the fact that the timescales for SS0.1 M are 2.2 days for condensation and 4.3 days for coagulation reveals a twofold difference in timescales between mass and number at the same supersaturation. The minimum timescales for SS1.0 N and SS0.1 N are 0.055 day (1.3 h) and 0.83 day (20 h), respectively, in the south of Beijing; these values are within the ranges of BC aging timescale estimated by *Riemer et al*. [2010] for an idealized urban plume (0.068–6.4 h and 11–54 h at supersaturations of 1% and 0.1%, respectively).

Figure 3 shows the diurnal variations of the BC aging timescale for condensation, coagulation, and the sum of condensation and coagulation. In East Asia, 03:00 to 05:00 universal time corresponds to around noon, and the timescales for condensation are smallest during this period (Figures 3a–3c) because the formation rate of

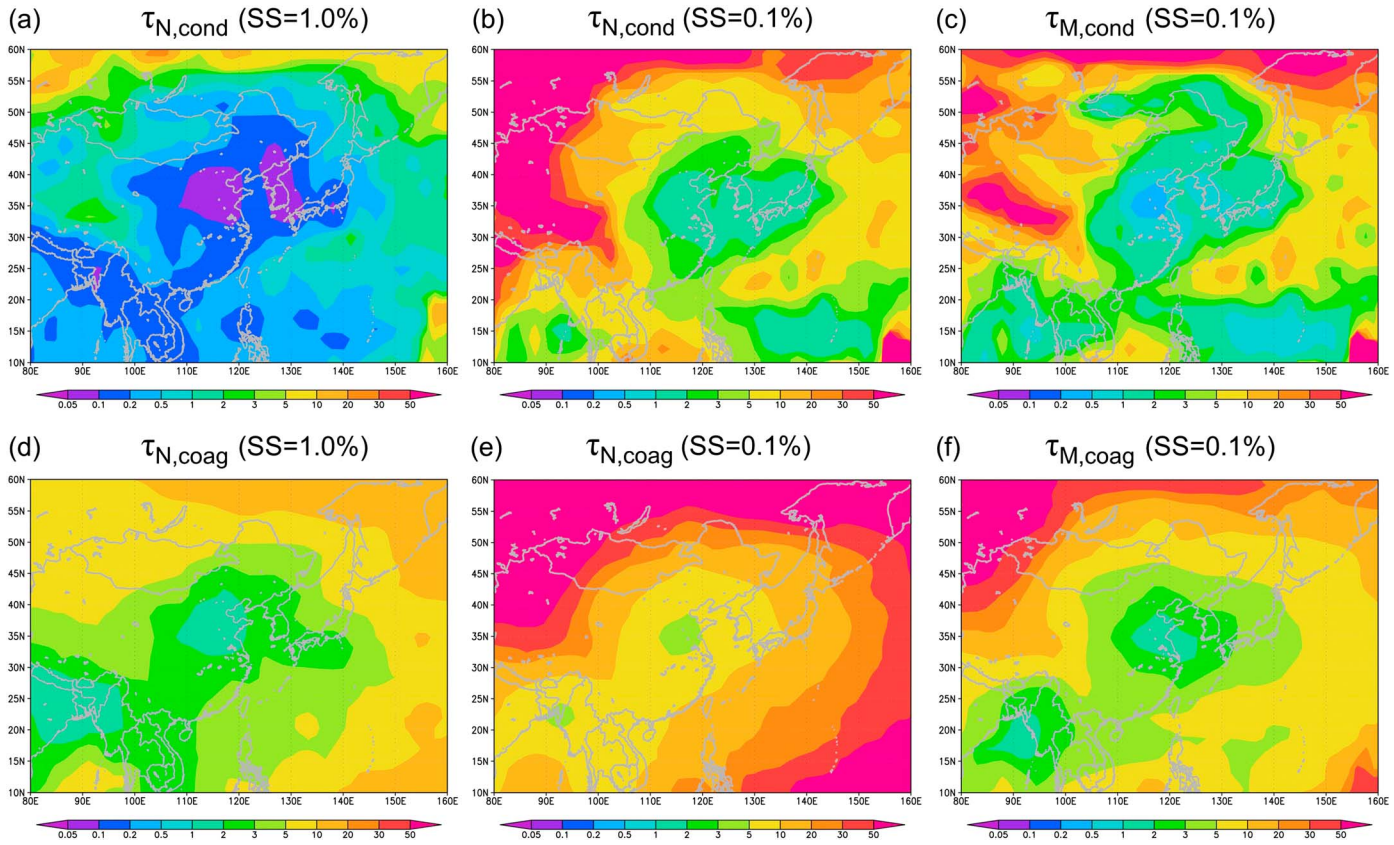

Figure 2. The distributions of the BC aging timescale (days) for (a–c) condensation and (d–f) coagulation processes at an altitude of 1 km during the simulation period. The BC aging timescales are shown for number concentrations of BC-containing particles at supersaturations of 1.0% (SS1.0 N) (a, d) and 0.1% (SS0.1 N) (b, e) and BC mass concentrations at a supersaturation of 0.1% (SS0.1 M) (c, f). The timescales are calculated using equations (1) and (2).

inorganic and organic aerosols are faster during the daytime. In contrast, the diurnal variations of the timescales for coagulation are small. The total (condensation + coagulation) aging timescales are smallest around noon.

The relative importance of condensation and coagulation processes depends on supersaturation over East Asia. Condensation is dominant throughout the day at a supersaturation of 1.0% (SS1.0 N) (Figure 3a). The timescales have diurnal variations of 0.08–0.6 day for condensation and 2.4–3.1 days for coagulation. The total aging timescale is determined primarily by the timescale for condensation. In contrast, both condensation and coagulation are important at a supersaturation of 0.1% (SS0.1 N and SS0.1 M) (Figures 3b and 3c). During the daytime, condensation is more important than coagulation to aging: the timescale for SS0.1 N is about 2 days for condensation and 9 days for coagulation. During the nighttime, coagulation is more important than condensation: the timescale for SS0.1 N is about 10 days for coagulation and 12 days for condensation. The contributions of condensation and coagulation are generally equivalent when averaged over 24 h: the timescale for SS0.1 N is 4.6 days for condensation and 9.5 days for coagulation (Table 1).

Table 1. Period- and Domain-Averaged BC Aging Timescale (Days) Simulated by ATRAS

Altitude	Parameter	Condensation	Coagulation	Condensation + Coagulation
1 km[a]	SS = 1.0%, Number	0.21 (0.23)	2.8 (3.8)	0.19 (0.22)
	SS = 0.1%, Number	4.6 (7.4)	9.5 (14.6)	3.1 (4.9)
	SS = 0.1%, Mass	2.2 (4.2)	4.3 (7.4)	1.5 (2.7)
5 km	SS = 1.0%, Number	1.1	4.7	0.90
	SS = 0.1%, Number	11.9	24.1	8.0
	SS = 0.1%, Mass	5.7	6.5	3.0

[a]The values in parentheses are the timescales simulated without organic aerosol formation processes.

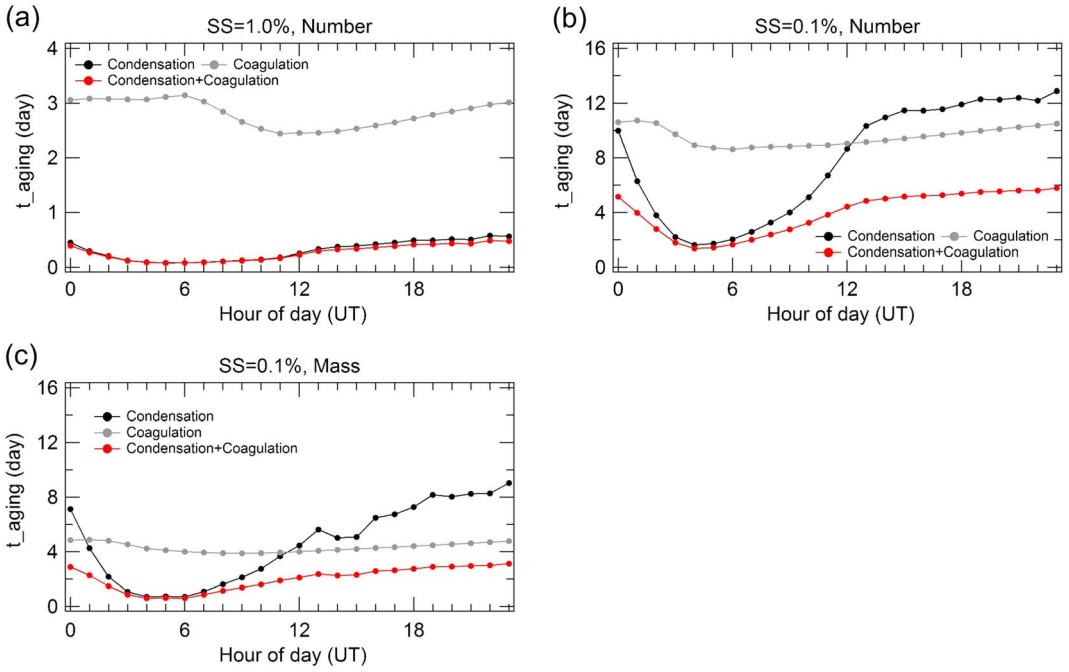

Figure 3. The diurnal variations of the BC aging timescale for (a) SS1.0 N, (b) SS0.1 N, and (c) SS0.1 M during the simulation period.

Figure 4 shows the vertical profiles of the BC aging timescale for SS1.0 N, SS0.1 N, and SS0.1 M. Overall, the timescale increases (the aging speed slows) with altitude for all parameters. The total aging timescales at 5 km are 0.9, 8.0, and 3.0 days for SS1.0 N, SS0.1 N, and SS0.1 M, respectively, and they are a factor of 2 to 5 higher than the corresponding timescales at an altitude of 1 km (Table 2). Though the absolute values of the timescales depend on altitude, the features of the timescales at 1 km are found at all altitudes over East Asia. At a supersaturation of 1.0%, condensation is more important than coagulation, and the total aging timescale is determined mostly by condensation at all altitudes (Figure 4a). At a supersaturation of 0.1%, both condensation and coagulation are important at all altitudes (Figures 4b and 4c). A size dependence of the aging timescale is also apparent at all altitudes: the timescale for number is higher than that for mass by a factor of 2 to 3 at all altitudes. The results show that the features obtained in this study are found from the surface to the upper troposphere in East Asia.

In summary, the variability of the BC aging timescale is larger spatially and temporally for condensation than for coagulation over East Asia (Figures 2–4). The absolute values of the BC aging timescale differed by more than an order of magnitude, depending on the choice of particle size (mass or number) and supersaturation (1.0% or 0.1%). These results suggest the importance of resolving the size and supersaturation dependence of

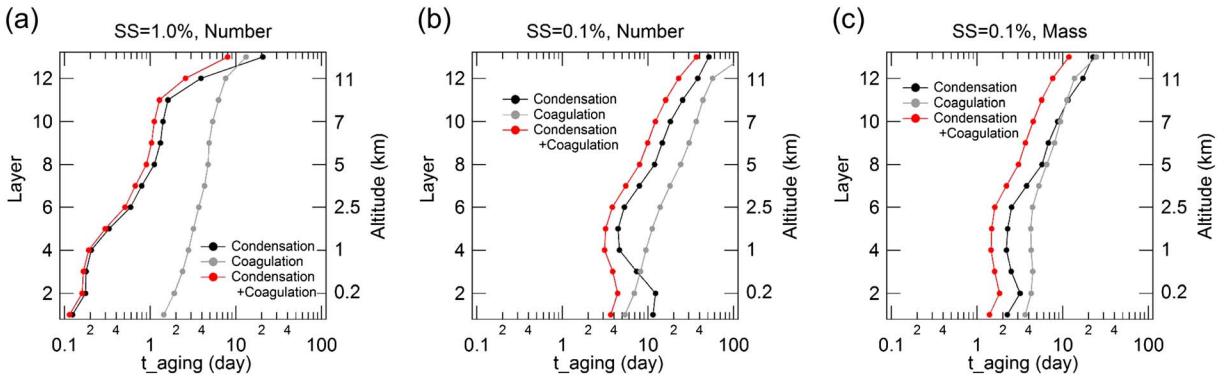

Figure 4. The vertical profiles of the BC aging timescale for (a) SS1.0 N, (b) SS0.1 N, and (c) SS0.1 M.

Table 2. CCN-Inactive BC Fraction (%) Simulated by ATRAS

Altitude	Parameter	Domain-Average	150 E
1 km[a]	SS = 1.0%, Number	3.4 (4.5)	1.2 (1.2)
	SS = 0.1%, Number	54.6 (63.2)	43.0 (49.9)
	SS = 0.1%, Mass	27.0 (31.8)	18.2 (19.7)
5 km	SS = 1.0%, Number	0.73	0.31
	SS = 0.1%, Number	45.9	39.1
	SS = 0.1%, Mass	18.2	14.5

[a]The values in parentheses are the fractions simulated without organic aerosol formation processes.

the BC aging timescale in aerosol models. The aging processes should not be modeled as a constant conversion rate from hydrophobic to hydrophilic for all BC particles.

4.2. CCN-Inactive BC Fraction

Next, the relationship between the BC aging timescale and the CCN activity of BC (CCN-inactive BC fraction) is clarified. The three-dimensional distributions of the CCN-inactive BC fraction are shown over East Asia and its outflow regions.

Figure 5 shows the distributions of the CCN-inactive BC fraction for SS1.0 N, SS0.1 N, and SS0.1 M at an altitude of 1 km. The fractions are generally higher over the Asian continent, and they gradually decrease with transport to the outflow regions. The reduction is probably due to aging processes during transport, but

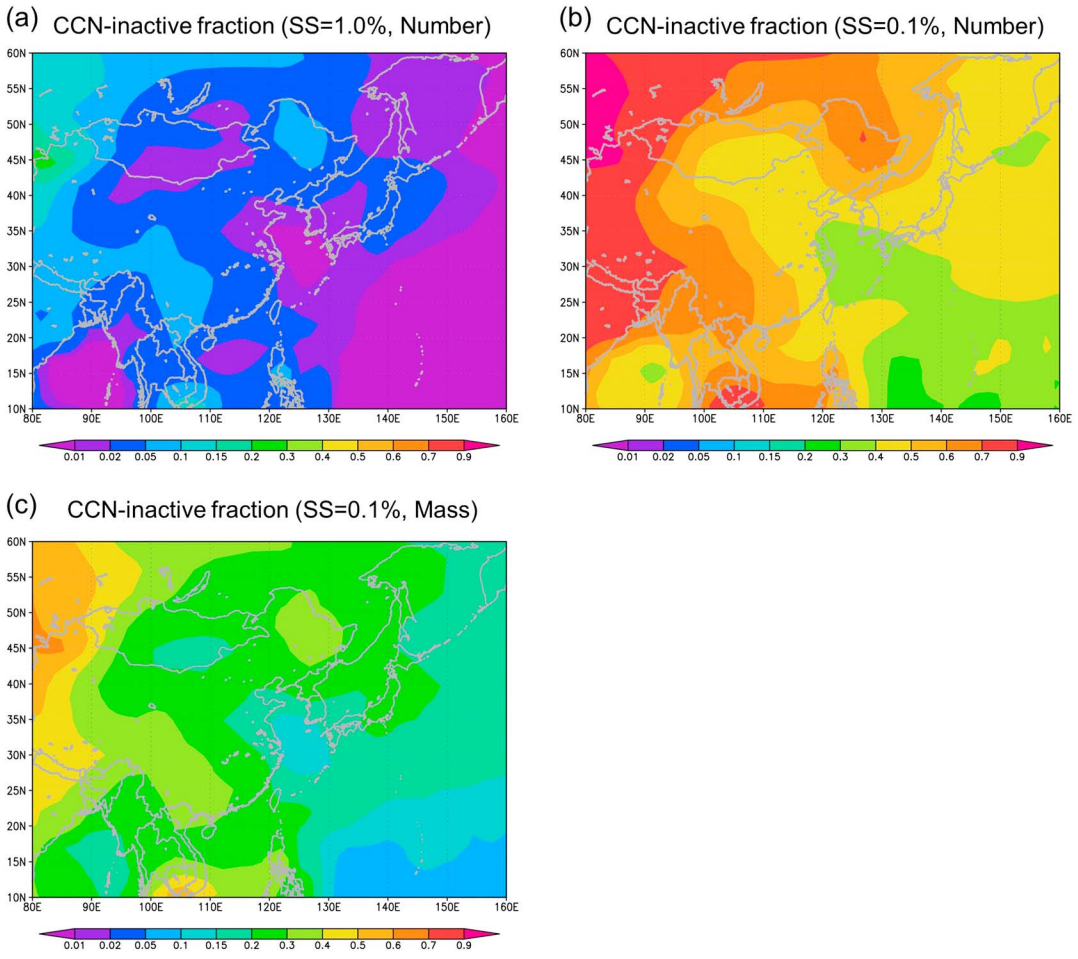

Figure 5. The distributions of the CCN-inactive BC fraction at an altitude of 1 km for (a) SS1.0 N, (b) SS0.1 N, and (c) SS0.1 M during the simulation period. The fractions are calculated by using equation (3).

the results in Figure 5 are obtained as the net effect of the aging processes and wet removal processes via precipitation. The aging processes decrease the CCN-inactive fraction, whereas wet removal processes increase the CCN-inactive fraction through selective removal of CCN-active particles.

The absolute values of the CCN-inactive fraction differed considerably between the parameters. Because the CCN-inactive BC fraction is only 3.4% for SS1.0 N (period and domain average), almost 100% of BC-containing particles are CCN-active at a supersaturation of 1.0%. In contrast, the CCN-inactive BC fraction is much larger at a supersaturation of 0.1%, and it is very size dependent; the CCN-inactive fractions are 55% and 27% for SS0.1 N and SS0.1 M, respectively (Table 2). The BC aging timescale is the highest (lowest) for SS0.1 N (SS1.0 N) (section 4.1), and a relatively slow (fast) aging speed leads to the largest (smallest) CCN-inactive BC fraction for SS0.1 N (SS1.0 N) over East Asia.

Table 2 shows the CCN-inactive BC fraction at 150°E. This longitude was chosen as representative of the outflow regions in East Asia. The dependence of the CCN-inactive BC fraction on size and supersaturation is clear at all latitudes and altitudes (Figures 5a–5c and Table 2). The average CCN-inactive BC fraction at 150°E is 1.2%, 43%, and 18% for SS1.0 N, SS0.1 N, and SS0.1 M, respectively, at 1 km (Table 2).

These results show that the activation of BC particles depends strongly on the size of aerosols and the maximum supersaturation in a cloud. The assumption that all BC-containing particles are CCN-active is valid in a cloud that has fast updraft velocity (high maximum supersaturation). However, this assumption is not correct in a cloud that has slow updraft velocity (low maximum supersaturation). In addition, in the latter case, the fraction of CCN-active BC particles has strong size dependence. These results suggest that BC models need to resolve the size and supersaturation dependence of the CCN activity of BC-containing particles to simulate BC concentrations and their distribution and lifetime more accurately.

4.3. Sensitivity of Organic Aerosol Formation

An important feature in the ATRAS model is to simulate both the BC mixing state and realistic organic aerosol concentrations in the atmosphere [*Matsui et al*., 2014b]. Considering this feature, this study evaluates the sensitivity of the BC aging timescale and the CCN-inactive BC fraction on organic aerosol formation processes. A sensitivity simulation without organic aerosol formation is conducted to quantify the sensitivity. In this simulation, only primary organic aerosols are considered, and they are assumed to be nonvolatile.

Because organic aerosol concentrations have previously been validated by surface measurements over the outflow regions in Japan [*Matsui et al*., 2014a, 2014b], this study focuses on the results near the surface (at an altitude of 1 km). When the organic aerosol formation processes are excluded, the total BC aging timescale (condensation + coagulation) changed from 0.19 to 0.22 day, from 3.1 to 4.9 days, and from 1.5 to 2.7 days for SS1.0 N, SS0.1 N, and SS0.1 M, respectively (Table 1). The changes in the BC aging timescale caused by organic aerosol formation lead to changes in the CCN-inactive fraction from 3.4% to 4.5%, from 55% to 63%, and from 27% to 32% for SS1.0 N, SS0.1 N, and SS0.1 M, respectively (Table 2). The impact of organic aerosol formation on these parameters is larger at a supersaturation of 0.1% than at a supersaturation of 1.0%. This result is consistent with the results of the study of *Matsui et al*. [2014a], which showed that organic aerosol formation increased CCN concentrations at lower supersaturations (larger particles) over East Asia. At a supersaturation of 0.1%, the BC aging timescale is enhanced by 60–80%, and this enhancement leads to an increase in the CCN-inactive fraction by 15–20% averaged over the domain and by 10–15% at 150°E.

Table 1 also shows that organic aerosol formation affects the BC aging timescale for both condensation and coagulation. A possible explanation of the influence on coagulation is that organic aerosol formation may change the production rate and the CCN activity of particles produced by coagulation via modification of the size and chemical composition of BC-containing particles.

4.4. Implication for Long-Range Transport

BC-containing particles age faster near the source areas (the timescale is less than 3 days for SS0.1 N), and the aging speed gradually slows with transport to the outflow regions (Figure 6a). The BC aging speed is much slower at 150°E; the BC aging timescale at this longitude is generally 5–20 days for SS0.1 N (Figure 6b) where BC concentrations are high (Figure 6c). Because the CCN-inactive BC fraction reaches 40% at 150°E for SS0.1 N (Figure 5b), the BC-containing particles could be transported long distances and for long times as CCN-

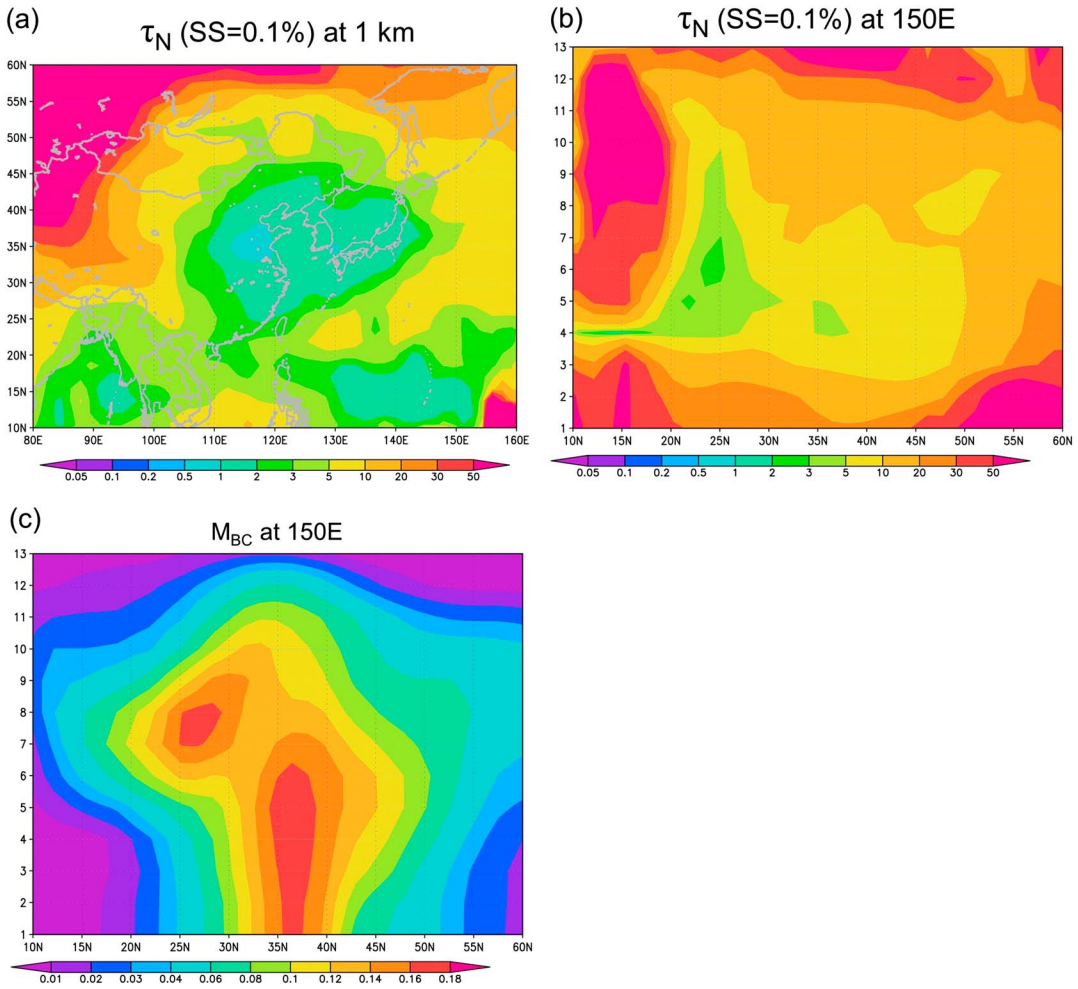

Figure 6. (a–b) The total (condensation + coagulation) BC aging timescale (days) for SS0.1 N (a) at an altitude of 1 km and (b) at 150°E during the simulation period. (c) The period-averaged BC mass concentrations ($\mu g\, m^{-3}$) at 150°E.

inactive particles because of the slow aging processes. BC particles in the free troposphere, in particular, would have a long lifetime because they would have few chances to experience cloud processes having high maximum supersaturation. These particles have the potential to play an important role in the transport of BC from East Asia to remote regions, such as North America and the Arctic.

This study cannot address the long-range transport of BC to remote regions directly because of the limitation of the simulation domains used in this study (section 3, Figure 3 of part 1). However, the importance of resolving the BC mixing state for the estimation of BC mass and its CCN activity is evaluated over the outflow regions (at 150°E) in section 4.5.

4.5. Importance of Mixing State Resolved Simulation

4.5.1. Offline Calculation

The BC concentrations in CCN-inactive particles are calculated in two ways by using the base simulation results with 12 × 10 (+8) aerosol bins. The first method is a calculation with full mixing-state-resolved information. The second method is an offline calculation without resolving mixing state by converting the information of 12 × 10 bins to 12 × 1 bins. In the second calculation, the mass and number concentrations are summed over the 10 mixing state bins, and the chemical composition (mixing state) is averaged for all particles in a size bin.

The total mass (each species) and number concentrations (the sum of all aerosol bins) are the same for the two calculations. Only the treatment of BC mixing state is different. The first calculation resolves pure BC, BC-free, and eight different internally mixed BC particles; the second calculation treats all particles as internally mixed BC with average chemical composition. BC mass concentrations are used in this section

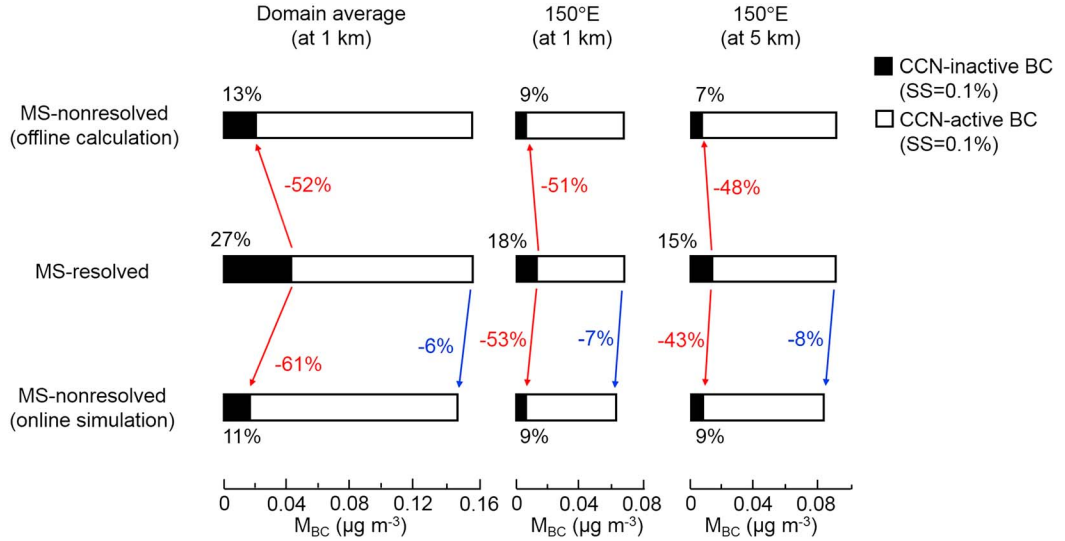

Figure 7. BC mass concentrations in the CCN-inactive (black) and CCN-active (white) particles (at a supersaturation of 0.1%) averaged (left) over the simulation domain and (middle and right) at 150°E during the simulation period. The results are shown for the simulation with resolving the BC mixing state (MS-resolved, middle), the offline calculation (section 4.5.1) without resolving the BC mixing state (MS-nonresolved, upper), and the online simulation (section 4.5.2) without resolving the BC mixing state (MS-nonresolved, lower). The black values show the fractions of the BC mass in the CCN-inactive particles to the total BC mass. The blue and red values show the changes in BC mass by not resolving the BC mixing state.

because the total BC mass concentrations are the same for the two calculations, whereas the total number concentrations of BC-containing particles are not the same.

The CCN-inactive BC fractions for SS0.1 M are estimated to be 27% and 13% for the mixing-state-resolved (MS-resolved, the first calculation) and the MS-nonresolved (the second offline calculation) calculations, respectively, averaged over the simulation domain (Figure 7). At 150°E, the fractions are 15–18% and 7–9% for the MS-resolved and the MS-nonresolved calculations, respectively (Figure 7). The CCN-inactive BC fractions are underestimated in the MS-nonresolved calculation because all particles are treated as internally mixed BC in the calculation. The BC mass in the CCN-inactive particles is underestimated by 50% over the simulation domain and at 150°E (Figure 7) in the calculation without resolving the BC mixing state. These underestimations underscore the importance of resolving the BC mixing state in model simulations for more accurate estimation of the CCN activity of BC particles over East Asia and its outflow regions.

4.5.2. Online Simulation

Next, the impact of resolving the BC mixing state is evaluated in terms of the total effect, including the transformation and removal processes of BC. A sensitivity simulation of the WRF-chem/ATRAS-MOSAIC model is conducted with 12 size × 1 mixing state bins (MS-nonresolved, size resolved only) during the simulation period (from 21 March to 26 April 2009). The simulation results are compared with the base simulation, which resolves the BC mixing state (MS-resolved, with 12 × 10 bins (+8 bins)).

Figure 7 shows BC mass concentrations in the CCN-active and CCN-inactive particles for both the MS-resolved and the MS-nonresolved online simulations. Total (CCN-active + CCN-inactive) BC mass concentrations differed between the simulations by 6% over the simulation domain and by 7–8% at 150°E. The MS-nonresolved simulation tends to underestimate total BC mass concentrations because the underestimation of the CCN-inactive BC mass (section 4.5.1) leads to an overestimation of BC removal.

Though total BC mass concentrations are not so different between the two simulations, the BC mass concentrations in the CCN-inactive particles have a much larger impact: they are underestimated by 60% over the simulation domain and by 40–50% at 150°E in the MS-nonresolved online simulation (Figure 8). Because BC aging timescale is very long at 150°E and eastward (>5–20 days, section 4.4), these results suggest that the impact of resolving the BC mixing state on BC mass will continue and become even greater during transport to remote regions such as North America and the Arctic through the selective

removal of CCN-active BC particles during transport. In fact, some global modeling studies have pointed out that BC concentrations over the Arctic are highly sensitive to the treatment of BC aging processes (e.g., conversion from hydrophobic to hydrophilic) and the resulting wet removal processes in their models [*Liu et al.*, 2011; *Vignati et al.*, 2010].

Many studies have been conducted to understand the importance of BC long-range transport from Asia to the Arctic, but the importance is not well quantified yet. Some studies have shown BC transport from Asia to the Arctic to be important [*Koch and Hansen*, 2005; *Wang et al.*, 2011], whereas some other studies have shown that the contribution of BC from Asia to the Arctic is limited [*Stohl*, 2006; *Matsui et al.*, 2011b, 2011c]. The results of this study suggest that it would be important to evaluate the transport of BC from sources in midlatitudes to remote regions using a model that can accurately represent BC aging processes and their dependence on particle size and supersaturation.

5. Summary and Conclusions

This study evaluated the aging timescale and the CCN activity of BC over East Asia and its outflow region during spring 2009 by using a size- and mixing-state-resolved three-dimensional model, WRF-chem/ATRAS-MOSAIC. The model explicitly calculated the changes in the BC mixing state due to BC aging processes such as condensation and coagulation, the enhancement of CCN activity by aging processes, and wet removal processes.

There was large spatial and temporal variability in the BC aging timescale over East Asia. The BC aging speed was relatively fast near the source regions and gradually slowed by 2 orders of magnitude during transport to the outflow regions. The BC aging timescale was strongly dependent on particle size and supersaturation; the timescales differed by more than an order of magnitude, depending on the choice of particle size (mass or number) and supersaturation (1.0% or 0.1%). The timescales were 0.19, 3.1, and 1.5 days for BC number at a supersaturation of 1.0%, BC number at a supersaturation of 0.1%, and BC mass at a supersaturation of 0.1%, respectively (period and domain average at an altitude of 1 km). Condensation was the dominant mechanism affecting BC aging at a supersaturation of 1.0%, whereas both condensation and coagulation were important at a supersaturation of 0.1%.

Due to the dependence of the BC aging timescale on size and supersaturation, the CCN activity of BC-containing particles was also very dependent on size and supersaturation. Almost 100% of BC-containing particles were CCN-active at a supersaturation of 1.0% over East Asia (the CCN-inactive BC fraction was 3.4% over the simulation domain at an altitude of 1 km), whereas more than half (55%) of BC-containing particles were CCN-inactive at a supersaturation of 0.1% over East Asia. The CCN-inactive fraction was also sensitive to particle size, and the fraction differed by a factor of 2 between mass (27%) and number (55%) concentrations at a supersaturation of 0.1%. These results suggest the importance of taking into consideration the size and supersaturation dependence of the aging timescale and the CCN activity of BC in aerosol models to simulate BC concentrations and their distribution and lifetime more accurately.

Because the BC aging timescale at 150°E and eastward was very long (longer than 5–20 days at 150°E and eastward for BC number at a supersaturation of 0.1%), CCN-inactive particles could be transported over long distances and times with a sufficiently slow conversion rate to CCN-active particles. These CCN-inactive particles therefore have a potential to play an important role in the transport of BC from East Asia to remote regions such as North America and the Arctic.

A sensitivity simulation without resolving BC mixing state (MS-nonresolved) underestimated total BC mass concentrations by 6% over the simulation domain and by 7–8% at 150°E, compared with the simulation resolving BC mixing state (MS-resolved). This is because all particles are treated as internally mixed BC in the MS-nonresolved simulation, whereas pure BC, BC-free, and eight different internally mixed BC particles are resolved in the MS-resolved simulation. Though total BC mass concentrations are not so different between the two simulations, the BC mass concentrations in the CCN-inactive particles have a much larger impact: they are underestimated by 60% over the simulation domain and by 40–50% at 150°E in the MS-nonresolved simulation. This result and the slow BC aging over the outflow region suggest that the impact of the BC mixing state treatment on BC concentrations will continue and become larger during transport to remote regions.

Acknowledgments

H. Matsui was supported by the Japan Society for the Promotion of Science (JSPS) Postdoctoral Fellowships for Research Abroad. This work was supported by the Ministry of Education, Culture, Sports, Science, and Technology and the Japan Society for the Promotion of Science (MEXT/JSPS) KAKENHI grants 26740014 and 26241003 and MEXT Green Network of Excellence (GRENE) and Arctic Challenge for Sustainability (ArCS) projects. This work was also supported by the environment research and technology development fund of the Ministry of the Environment, Japan (2–1403). The model simulations were conducted using the MSTSC super computer system at the Japan Agency for Marine-Earth Science and Technology. Data can be obtained by contacting H. Matsui (matsui@nagoya-u.jp). The author would like to thank the two anonymous reviewers of this manuscript for their useful and helpful suggestions.

References

Abdul-Razzak, H., and S. J. Ghan (2000), A parameterization of aerosol activation: 2. Multiple aerosol types, *J. Geophys. Res.*, *105*(D5), 6837–6844, doi:10.1029/1999JD901161.

Bond, T. C., et al. (2013), Bounding the role of black carbon in the climate system: A scientific assessment, *J. Geophys. Res. Atmos.*, *118*, 5380–5552, doi:10.1002/jgrd.50171.

Boucher, O., et al. (2013), Clouds and aerosols, in *Climate Change 2013: The Physical Science Basis. Contribution of Working Group I to the Fifth Assessment Report of the Intergovernmental Panel on Climate Change*, edited by T. F. Stocker et al., Cambridge Univ. Press, Cambridge, U. K., and New York.

Chen, W.-T., Y. H. Lee, P. J. Adams, A. Nenes, and J. H. Seinfeld (2010), Will black carbon mitigation dampen aerosol indirect forcing?, *Geophys. Res. Lett.*, *37*, L09801, doi:10.1029/2010GL042886.

Cooke, W. F., V. Ramaswamy, and P. Kasibhatla (2002), A general circulation model study of the global carbonaceous aerosol distribution, *J. Geophys. Res.*, *107*(D16), 4279, doi:10.1029/2001JD001274.

Croft, B., U. Lohmann, and K. von Salzen (2005), Black carbon ageing in the Canadian Center for Climate modelling and analysis atmospheric general circulation model, *Atmos. Chem. Phys.*, *5*, 1931–1949.

Easter, R. C., S. J. Ghan, Y. Zhang, R. D. Saylor, E. G. Chapman, N. S. Laulainen, H. Abdul-Razzak, L. R. Leung, X. Bian, and R. A. Zaveri (2004), MIRAGE: Model description and evaluation of aerosols and trace gases, *J. Geophys. Res.*, *109*, D20210, doi:10.1029/2004JD004571.

Fahey, K. M., and S. N. Pandis (2001), Optimizing model performance: Variable size resolution in cloud chemistry modeling, *Atmos. Environ.*, *35*, 4471–4478.

Fast, J. D., W. I. Gustafson Jr., R. C. Easter, R. A. Zaveri, J. C. Barnard, E. G. Chapman, G. A. Grell, and S. E. Peckham (2006), Evolution of ozone, particulates, and aerosol direct radiative forcing in the vicinity of Houston using a fully coupled meteorology-chemistry-aerosol model, *J. Geophys. Res.*, *111*, D21305, doi:10.1029/2005JD006721.

Fierce, L., N. Riemer, and T. C. Bond (2015), Explaining variance in black carbon's aging timescale, *Atmos. Chem. Phys.*, *15*, 3173–3191.

Grell, G. A., S. E. Peckham, R. Schmitz, S. A. McKeen, G. Frost, W. C. Skamarock, and B. Eder (2005), Fully coupled "online" chemistry within the WRF model, *Atmos. Environ.*, *39*, 6957–6975.

Guenther, A., T. Karl, P. Harley, C. Wiedinmyer, P. I. Palmer, and C. Geron (2006), Estimates of global terrestrial isoprene emissions using MEGAN (Model of Emissions of Gases and Aerosols from Nature), *Atmos. Chem. Phys.*, *6*, 3181–3210.

Hansen, J., and L. Nazarenko (2004), Soot climate forcing via snow and ice albedos, *Proc. Natl. Acad. Sci. U.S.A.*, *101*(2), 423–428.

Huang, L., S. L. Gong, C. Q. Jia, and D. Lavoué (2010), Relative contributions of anthropogenic emissions to black carbon aerosol in the Arctic, *J. Geophys. Res.*, *115*, D19208, doi:10.1029/2009JD013592.

Jacobson, M. Z. (1997), Development and application of a new air pollution, modeling system–II. Aerosol module structure and design, *Atmos. Environ.*, *31*, 131–144.

Johnson, B. T., K. P. Shine, and P. M. Forster (2004), The semidirect aerosol effect: Impact of absorbing aerosols on marine stratocumulus, *Q. J. R. Meteorol. Soc.*, *130*(599), 1407–1422.

Koch, D., and A. D. Del Genio (2010), Black carbon semi-direct effects on cloud cover: Review and synthesis, *Atmos. Chem. Phys.*, *10*, 7685–7696.

Koch, D., and J. Hansen (2005), Distant origins of Arctic black carbon: A Goddard Institute for Space Studies ModelE experiment, *J. Geophys. Res.*, *110*, D04204, doi:10.1029/2004JD005296.

Koch, D., et al. (2009), Evaluation of black carbon estimations in global aerosol models, *Atmos. Chem. Phys.*, *9*, 9001–9026.

Kondo, Y., N. Oshima, M. Kajino, R. Mikami, N. Moteki, N. Takegawa, R. L. Verma, Y. Kajii, S. Kato, and A. Takami (2011), Emissions of black carbon in East Asia estimated from observations at a remote site in the East China Sea, *J. Geophys. Res.*, *116*, D16201, doi:10.1029/2011JD015637.

Kulmala, M., K. E. J. Lehtinen, and A. Laaksonen (2006), Cluster activation theory as an explanation of the linear dependence between formation rate of 3 nm particles and sulphuric acid concentration, *Atmos. Chem. Phys.*, *6*, 787–793.

Liu, J., S. Fan, L. W. Horowitz, and H. Levy II (2011), Evaluation of factors controlling long-range transport of black carbon to the Arctic, *J. Geophys. Res.*, *116*, D04307, doi:10.1029/2010JD015145.

Matsui, H. (2016), Black carbon simulations using a size- and mixing-state-resolved three-dimensional model: 1. Radiative effects and their uncertainties, *J. Geophys. Res. Atmos.*, *121*, doi:10.1002/2015JD023998.

Matsui, H., M. Koike, Y. Kondo, N. Takegawa, A. Wiedensohler, J. D. Fast, and R. A. Zaveri (2011a), Impact of new particle formation on the concentrations of aerosols and cloud condensation nuclei around Beijing, *J. Geophys. Res.*, *116*, D19208, doi:10.1029/2011JD016025.

Matsui, H., et al. (2011b), Seasonal variation of the transport of black carbon aerosol from the Asian continent to the Arctic during the ARCTAS aircraft campaign, *J. Geophys. Res.*, *116*, D05202, doi:10.1029/2010JD015067.

Matsui, H., et al. (2011c), Accumulation-mode aerosol number concentrations in the Arctic during the ARCTAS aircraft campaign: Long-range transport of polluted and clean air from the Asian continent, *J. Geophys. Res.*, *116*, D20217, doi:10.1029/2011JD016189.

Matsui, H., M. Koike, Y. Kondo, N. Moteki, J. D. Fast, and R. A. Zaveri (2013a), Development and validation of a black carbon mixing state resolved three-dimensional model: Aging processes and radiative impact, *J. Geophys. Res. Atmos.*, *118*, 2304–2326, doi:10.1029/2012JD018446.

Matsui, H., M. Koike, N. Takegawa, Y. Kondo, A. Takami, T. Takamura, S. Yoon, S.-W. Kim, H.-C. Lim, and J. D. Fast (2013b), Spatial and temporal variations of new particle formation in East Asia using an NPF-explicit WRF-chem model: North–south contrast in new particle formation frequency, *J. Geophys. Res. Atmos.*, *118*, 11,647–11,663, doi:10.1002/jgrd.50821.

Matsui, H., M. Koike, Y. Kondo, J. D. Fast, and M. Takigawa (2014a), Development of an aerosol microphysical module: Aerosol Two-dimensional bin module for foRmation and Aging Simulation (ATRAS), *Atmos. Chem. Phys.*, *14*, 10,315–10,331.

Matsui, H., M. Koike, Y. Kondo, A. Takami, J. D. Fast, Y. Kanaya, and M. Takigawa (2014b), Volatility basis-set approach simulation of organic aerosol formation in East Asia: Implications for anthropogenic–biogenic interaction and controllable amounts, *Atmos. Chem. Phys.*, *14*, 9513–9535.

Moteki, N., Y. Kondo, N. Oshima, N. Takegawa, M. Koike, K. Kita, H. Matsui, and M. Kajino (2012), Size dependence of wet removal of black carbon aerosols during transport from the boundary layer to the free troposphere, *Geophys. Res. Lett.*, *39*, L13802, doi:10.1029/2012GL052034.

Myhre, G., et al. (2013), Anthropogenic and natural radiative forcing, in *Climate Change 2013: The Physical Science Basis. Contribution of Working Group I to the Fifth Assessment Report of the Intergovernmental Panel on Climate Change*, edited by T. F. Stocker et al., Cambridge Univ. Press, Cambridge, U. K., and New York.

Oshima, N., and M. Koike (2013), Development of a parameterization of black carbon aging for use in general circulation models, *Geosci. Model. Dev.*, *6*, 263–282.

Oshima, N., M. Koike, Y. Zhang, and Y. Kondo (2009), Aging of black carbon in outflow from anthropogenic sources using a mixing state resolved model: 2. Aerosol optical properties and cloud condensation nuclei activities, *J. Geophys. Res.*, *114*, D18202, doi:10.1029/2008JD011681.

Oshima, N., et al. (2012), Wet removal of black carbon in Asian outflow: Aerosol Radiative Forcing in East Asia (A-FORCE) aircraft campaign, *J. Geophys. Res.*, *117*, D03204, doi:10.1029/2011JD016552.

Petters, M. D., and S. M. Kreidenweis (2007), A single parameter representation of hygroscopic growth and cloud condensation nucleus activity, *Atmos. Chem. Phys.*, *7*, 1961–1971.

Ramanathan, V., P. J. Crutzen, J. T. Kiehl, and D. Rosenfeld (2001), Aerosols, climate, and the hydrological cycle, *Science*, *294*(5549), 2119–2124.

Riemer, N., H. Vogel, and B. Vogel (2004), Soot aging time scales in polluted regions during day and night, *Atmos. Chem. Phys.*, *4*, 1885–1893.

Riemer, N., M. West, R. A. Zaveri, and R. C. Easter (2009), Simulating the evolution of soot mixing state with a particle-resolved aerosol model, *J. Geophys. Res.*, *114*, D09202, doi:10.1029/2008JD011073.

Riemer, N., M. West, R. A. Zaveri, and R. C. Easter (2010), Estimating soot aging time scales with a particle-resolved aerosol model, *J. Aerosol Sci.*, *41*, 143–158.

Shindell, D. T., et al. (2008), A multi-model assessment of pollution transport to the Arctic, *Atmos. Chem. Phys.*, *8*, 5353–5372.

Simmel, M., and S. Wurzler (2006), Condensation and activation in sectional cloud microphysical models, *Atmos. Res.*, *80*, 218–236.

Skamarock, W. C., J. B. Klemp, J. Dudhia, D. O. Gill, D. M. Barker, W. Wang, and J. G. Powers (2008), A description of the advanced research WRF version 3, NCAR Tech. Note, NCAR/TN-475 + STR, Natl. Cent. Atmos. Res., Boulder, Colo.

Stier, P., J. H. Seinfeld, S. Kinne, J. Feichter, and O. Boucher (2006), Impact of nonabsorbing anthropogenic aerosols on clear-sky atmospheric absorption, *J. Geophys. Res.*, *111*, D18201, doi:10.1029/2006JD007147.

Stohl, A. (2006), Characteristics of atmospheric transport into the Arctic troposphere, *J. Geophys. Res.*, *111*, D11306, doi:10.1029/2005JD006888.

Streets, D. G., et al. (2003), An inventory of gaseous and primary aerosol emissions in Asia in the year 2000, *J. Geophys. Res.*, *108*(D21), 8809, doi:10.1029/2002JD003093.

Takami, A., T. Miyoshi, A. Shimono, and S. Hatakeyama (2005), Chemical composition of fine aerosol measured by AMS at Fukue Island, Japan, during APEX period, *Atmos. Environ.*, *39*, 4913–4924.

Takami, A., T. Miyoshi, A. Shimono, N. Kaneyasu, S. Kato, Y. Kajii, and S. Hatakeyama (2007), Transport of anthropogenic aerosols from Asia and subsequent chemical transformation, *J. Geophys. Res.*, *112*, D22S31, doi:10.1029/2006JD008120.

van der Werf, G. R., J. T. Randerson, L. Giglio, G. J. Collatz, M. Mu, P. S. Kasibhatla, D. C. Morton, R. S. DeFries, Y. Jin, and T. T. van Leeuwen (2010), Global fire emissions and the contribution of deforestation, savanna, forest, agricultural, and peat fires (1997 – 2009), *Atmos. Chem. Phys.*, *10*, 11,707–11,735.

Vignati, E., M. Karl, M. Krol, J. Wilson, P. Stier, and F. Cavalli (2010), Sources of uncertainties in modelling black carbon at the global scale, *Atmos. Chem. Phys.*, *10*, 2595–2611.

Wang, Q., et al. (2011), Sources of carbonaceous aerosols and deposited black carbon in the Arctic in winter-spring: Implications for radiative forcing, *Atmos. Chem. Phys.*, *11*, 12,453–12,473.

Zaveri, R. A., R. C. Easter, J. D. Fast, and L. K. Peters (2008), Model for simulating aerosol interactions and chemistry (MOSAIC), *J. Geophys. Res.*, *113*, D13204, doi:10.1029/2007JD008782.

Zaveri, R. A., J. C. Barnard, R. C. Easter, N. Riemer, and M. West (2010), Particle-resolved simulation of aerosol size, composition, mixing state, and the associated optical and cloud condensation nuclei activation properties in an evolving urban plume, *J. Geophys. Res.*, *115*, D17210, doi:10.1029/2009JD013616.